Published in Optics Letters 31, issue 4, 513-515, 2006
which should be used for any reference to this work

Optically tunable microcavity in a planar photonic crystal silicon waveguide buried in oxide

Iwan Märki, Martin Salt, and Hans Peter Herzig

Institute of Microtechnology, University of Neuchâtel, Rue A.-L. Breguet 2, CH-2000 Neuchâtel, Switzerland

Ross Stanley

Centre Suisse d'Electronique et de Microtechnique SA, Rue Jaquet-Droz 1, CH-2007 Neuchâtel, Switzerland

L. El Melhaoui, P. Lyan, and J. M. Fedeli

Laboratoire d'Electronique de Technologie de l'Information, CEA-Grenoble, 17 Rue des Martyrs, 38 054 Grenoble Cedex 9, France

We present all-optical tuning and switching of a microcavity inside a two-dimensional photonic crystal waveguide. The photonic crystal structure is fabricated in silicon-on-insulator using complementary metal-oxide semiconductor processing techniques based on deep ultraviolet lithography and is completely buried in a silicon dioxide cladding that provides protection from the environment. By focusing a laser onto the microcavity region, both a thermal and a plasma dispersion effect are generated, allowing tuning and fast modulation of the in-plane transmission. By means of the temporal characteristics of the in-plane transmission, we experimentally identify a slower thermal and a fast plasma dispersion effect with modulation bandwidths of the order of several 100 kHz and up to the gigahertz level, respectively.

The ability to control light propagation on a wavelength scale by use of silicon planar photonic crystal structures is well known. Planar photonic crystal waveguides, bends, and microcavities are considered basic building blocks for applications such as microlasers, filters, multiplexers, and optical switches.[1–4] It is possible to tune or switch photonic crystal devices in various ways, for example, by control of temperature,[5] refractive index change using liquid crystals,[6] control of free charge carrier density,[7] or nonlinear material effects.[8] Active photonic crystal devices allow further miniaturization of integrated optical circuits with active functionality. High-Q microcavities in planar photonic crystals exhibit highly localized fields and narrow transmission bands.[9] Even a small perturbation of the localized field can change the transmission properties of the microcavity. The relatively weak nonlinear properties of silicon can be used in these structures for low-power modulation and switching.[10–12]

Until now most of the work done on tuning and modulating silicon photonic crystal devices has been based on an electrically controlled thermo-optical effect. In this work, we present an optically tunable microcavity inside a photonic crystal waveguide. We show experimentally that tuning the resonant wavelength and modulating the transmission signal is possible by using a laser focused onto the microcavity region, generating both thermal and plasma dispersion effects. As silicon membranes are delicate and thus sensitive to the environment, our waveguide structures are fully buried in a silicon dioxide cladding being protected and more practical for many applications, notwithstanding the smaller refractive index contrast.

The design of the in-plane resonant cavity is shown in Fig. 1. The photonic crystal consists of a triangular array of cylindrical holes in a thin silicon layer. The silicon slab is completely buried in a silicon dioxide cladding and is therefore protected from the environment. The in-plane resonant cavity is formed by two identical one-dimensional Bragg reflectors inside the photonic crystal waveguide and has a length of ~330 nm. The cavity structure is designed to yield a highly localized optical field inside the cavity and high in-plane transmission for a narrow frequency band. For ease of fabrication, we have kept the design as simple as possible while accepting lower performance for the cavity. Thus, the holes of the one-dimensional Bragg reflectors are all equally spaced

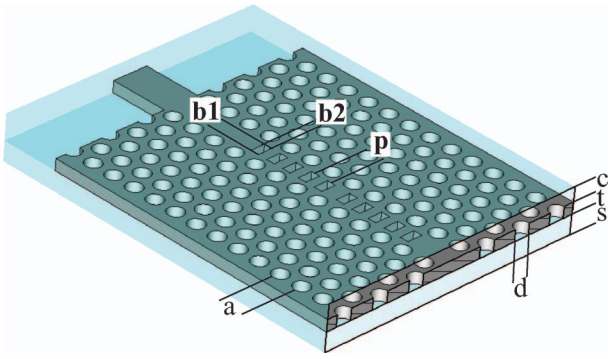

Fig. 1. In-plane photonic crystal microcavity structure buried in silicon dioxide (PhC period $a=490$ nm, hole diameter $d=350$ nm, core thickness $t=238$ nm, bottom oxide thickness $s\approx2000$ nm, upper cladding thickness $c\approx700$ nm). The microcavity inside the photonic crystal waveguide is formed by two five-hole Bragg reflectors (hole dimensions b1=325 nm and b2=180 nm, period $p=373$ nm).

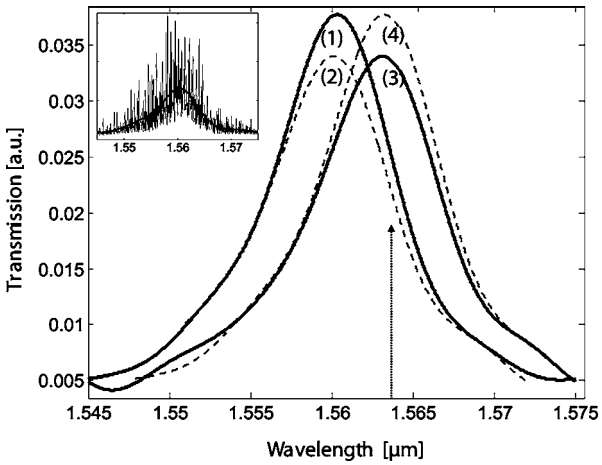

Fig. 2. Measured transmission spectra through the photonic crystal microcavity (1) without and (3) with the control laser illumination ($\lambda = 532$ nm). Curves (2) and (4) approximately indicate the change induced by the plasma dispersion and thermo-optical effects, respectively. The arrow indicates the fixed wavelength for the temporal response measurements. The inset depicts the unfiltered transmission spectrum with the periodic Fabry–Perot interference oscillations.

and have the same dimensions. The designed photonic crystal microcavity structure was fabricated by the Laboratoire d'Electronique de Technologie de l'Information, France, using deep ultraviolet lithography at a wavelength of 193 nm. After the lithography process, the patterns in the photoresist are transferred into the silicon layer of a silicon-insulator wafer by use of HBr dry etching technology via a silicon dioxide hard mask. As a final step, the etched structures in the silicon are then covered with an oxide layer.

The transmission measurements are performed using a tunable laser source. By means of an aspheric lens, TE-polarized light (in-plane polarization) is injected into a 10 μm wide silicon waveguide. The light is guided through a taper, which reduces the waveguide width to 0.5 μm, to the photonic crystal waveguide. For a narrow frequency band the light propagating in the photonic crystal waveguide couples into the resonant cavity, where it is highly localized and eventually transmitted. With a second, identical taper the transmitted light is then guided to the exit of the device, where it is collected by a microscope objective and focused onto an InGaAs detector for measurements.

The measured transmission spectrum of the microcavity exhibits a resonance peak at a wavelength of 1.561 μm with an approximate maximum transmission efficiency of 11%. The quality factor is of the order of 200. Further transmission and loss properties of the microcavity were discussed in Ref. 13.

At the transmission resonance the spectral frequency response of the microcavity is sensitive to the smallest perturbations of the region around the localized field. To induce a perturbation, a laser with a wavelength of $\lambda = 532$ nm and a maximum power of 30 mW is focused onto the center of the microcavity. The light is strongly absorbed ($\sim 30\%$) by the silicon core of the waveguide, whereas the upper and lower oxide claddings are transparent for the control laser wavelength. Figure 2 shows the measured transmission spectra through the microcavity [curve (1)] without and [curve (3)] with the control laser turned on. The raw measurement data have been numerically smoothed to remove the periodic Fabry–Perot interference (compare with the inset in Fig. 2), which is due to the reflection at the input and output waveguide end facets. The resonant wavelength is redshifted by 3 nm, and the transmission is attenuated by approximately 10% due to thermo-optical and plasma dispersion effects.

To distinguish the different physical effects we observe the temporal response of the transmission signal when a square modulation pulse of 12 μs is applied to the control laser, shown in Fig. 3. A wavelength of $\lambda = 1.564$ μm, slightly above the resonant wavelength (the peak wavelength of the thermally shifted transmission spectrum, see Fig. 2), was chosen for the transmitted light to conveniently observe both the thermo-optical and the plasma dispersion effects in the modulated transmission signal. The switching time of the control laser is of the order of 100 ns. Coinciding with the switch-on of the control laser, we observe a small negative peak [position (2) in Fig. 3], which is due to the fast plasma dispersion effect inducing a small negative index change and an increase in the absorption coefficient. Following, the transmission efficiency increases with a rise time of ~ 5 μs as a result of the slower thermo-optical effect [position (3)], which induces a positive index change, shifting the resonant wavelength toward the wavelength of the transmission signal. At the switch-off of the probe laser a small positive peak is observed [position (4)]. This peak is due to the recombination of the free carriers, which increases the refractive index and reduces the absorption coefficient slightly. Sequentially, the transmission properties return to the initial state with thermal relaxation. For a better understanding of the present

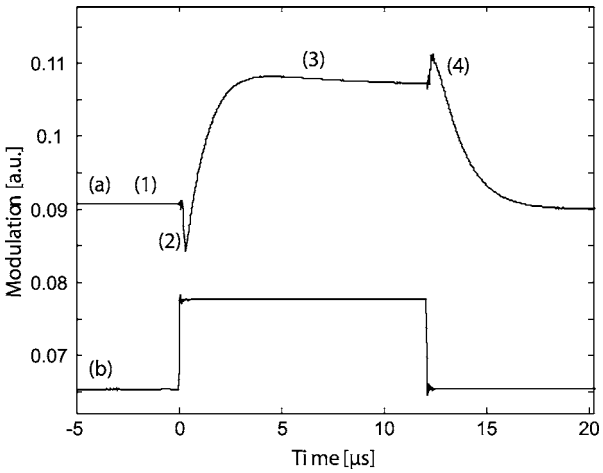

Fig. 3. (a) Measured temporal response of the transmission signal with its switching characteristics [positions (1) to (4)]. The slight decrease of the signal in position (3) is most likely due to secondary thermal effects induced in the bulk silicon. (b) Square modulation pulse applied to the control laser.

effects the consecutive change in the transmission properties can be indicated in Fig. 2 according to the observed temporal response. The arrow in Fig. 2 marks the fixed wavelength of $\lambda = 1.564$ μm. The dotted curve (2) corresponding to position (2) in Fig. 3 approximately indicates the change induced by the plasma dispersion effect alone, whereas the dotted curve (4) corresponding to position (4) in Fig. 3 approximately indicates the change due to the thermo-optical effect.

From these measurements, the size of the thermo-optical and plasma dispersion effects can be estimated. Three-dimensional simulations show that a change of $\Delta n = +0.05$ in the refractive index of the silicon layer gives the required redshift. For silicon, dn/dT is $1.86 \pm 0.08 \times 10^{-4}$/K at 1.55 μm,[14] indicating a local temperature rise of 270 °C due to the thermo-optical effect. The observed attenuation of approximately 10% is due to the presence of free carriers generated by the plasma dispersion effect. Assuming an approximate effective cavity length of $Q \times L_{\text{cavity}}$, the absorption coefficient is of the order of 15 cm^{-1}. Based on the Drude model,[15] the induced charge density is estimated to be $\Delta N \approx 10^{18}$ cm^{-3}, causing a refractive index change of approximately $\Delta n = -0.0007$, which is more than one order of magnitude smaller than the thermo-optically induced index change. This explains the observed redshift in the transmission spectrum.

Furthermore, from Fig. 3, we estimate the thermo-optical maximum modulation frequency to be of the order of 200 kHz. Below this frequency a modulation depth of ~30% can be achieved (see Fig. 2). The plasma dispersion effect allows much greater modulation frequencies. We measured the transmitted signal modulated at 50 MHz working above the thermal maximum modulation frequency. For modulation of the control laser an electro-optical resonant modulator was used, limiting the maximum modulation frequency to 50 MHz. In this case, the modulation depth is reduced to ~10% owing to the weaker plasma dispersion effect and to the diminished modulation depth of the control laser. A relaxation time for free carriers in a different light-confining structure on silicon has been measured to be of the order of 500 ps.[16,17] Therefore, modulation frequencies in the gigahertz range should be possible.

A higher Q factor and transmission efficiency would allow a reduction in the power of the control laser and an increase in the maximum modulation frequency, improving the performance of the photonic crystal optical modulator. The differing temporal response of the thermal and plasma dispersion effects should allow simultaneous tuning and high-speed modulation in a limited range, increasing functionality. Based on the plasma dispersion effect, dense integration of several structures not suffering from the thermal cross-talk encountered in present-day integrated optical devices becomes possible. With current technology one could envision the integration of the control laser source onto the same chip, by stacking a wafer-based laser aligned with a wafer-based waveguide. Alternatively, integration of the optical tuning and the modulation method into a completely planar solution by use of a different wavelength for the control laser (slightly different from the wavelength of the transmission signal) could be realized with two intersecting resonant cavities. This configuration would permit modulation because of the free-carrier-induced change of the refractive index based on two-photon absorption.

In conclusion, we have demonstrated that high-speed optical switching and resonant wavelength tuning on the subwavelength scale are achievable with a relatively simple technique. The induced thermal and plasma dispersion effects have been clearly identified by means of the temporal characteristics of the transmission signal. These results indicate that an improved design based on the device presented could serve as a basic component of high-speed all-optical integrated circuits based on silicon photonic crystal structures with applications in, for example, high-bandwidth data routing.

I. Märki's e-mail address is iwan.maerki@unine.ch.

References

1. A. Mekis, J. C. Chen, I. Kurland, S. Fan, P. Villeneuve, and J. D. Joannopoulos, Phys. Rev. Lett. **77**, 3787 (1996).
2. S. Noda, M. Imada, M. Okano, S. Ogawa, M. Mochizuki, and A. Chutinan, IEEE J. Quantum Electron. **38**, 726 (2002).
3. M. Lončar, T. Yoshie, A. Scherer, P. Gogna, and Y. Qiu, Appl. Phys. Lett. **81**, 2680 (2002).
4. M. Notomi, A. Shinya, S. Mitsugi, E. Kuramochi, and H.-Y. Ryu, Opt. Express **12**, 1551 (2004).
5. E. A. Camargo, H. M. H. Chong, and R. M. De La Rue, Opt. Express **12**, 588 (2004).
6. Ch. Schuller, F. Klopf, J. P. Reithmaier, M. Kamp, and A. Forchel, Appl. Phys. Lett. **82**, 2767 (2003).
7. S. W. Leonard, H. M. van Driel, J. Schilling, and R. B. Wehrsporn, Phys. Rev. B **66**, 161102 (2002).
8. A. Locatelli, D. Modotto, D. Paloschi, and C. De Angelis, Opt. Commun. **237**, 97 (2004).
9. Y. Akahane, T. Asano, B.-S. Song, and S. Noda, Nature **425**, 944 (2003).
10. V. R. Almeida, C. A. Barrios, R. R. Panepucci, and M. Lipson, Nature **31**, 1081 (2004).
11. V. R. Almeida and M. Lipson, Opt. Lett. **29**, 2387 (2004).
12. P. E. Barclay, K. Srinivasan, and O. Painter, Opt. Express **13**, 801 (2005).
13. I. Märki, M. Salt, H. P. Herzig, R. Stanley, L. E. Melhaoui, P. Lyan, and J. M. Fedeli, J. Appl. Phys. **98**, 013103 (2005).
14. G. Cocorullo and I. Rendina, Electron. Lett. **28**, 83 (1992).
15. R. A. Soref and B. R. Bennet, IEEE J. Quantum Electron. **QE-23**, 123 (1987).
16. M. Lipson, Nanotechnology **15**, 622 (2004).
17. V. R. Almeida and M. Lipson, Opt. Lett. **29**, 2387 (2004).